Isoelectronic Doping in Tin Oxide by Ge Leading to Mobility Increase of Hole and Electron: Experiments and DFT Simulation

Jay Singh*
Department of Electronics and Communication Engineering
Indian Institute of Technology Roorkee
Uttarakhand 247 667, India

Suman Gora*
Department of Electronics and Communication Engineering
Indian Institute of Technology Roorkee
Uttarakhand 247 667, India {*Equally contributed}

Arnab Datta#
Department of Electronics and Communication Engineering
Indian Institute of Technology Roorkee
Uttarakhand 247 667, India (# Email: arnab.datta@ece.iitr.ac.in)

***Abstract*— Mobility enhancement in sputter deposited tin oxide due to its isoelectronic doping by germanium (Ge) is investigated here by experiments, which was validated by DFT simulation. Ge doping (20 W Ge target power) increased hole mobility to 4.81 cm^2/V-s and electron to 16.86 cm^2/V-s, which were attributed to higher orbital overlap between the Sn s and Ge s orbitals**

Keywords*— *Tin Oxide, Ge doping, Mobility, DFT Simulation

I. Introduction

High-mobility metal-oxide-based transparent conducting oxides (TCOs) are the suitable materials for thin-film transistors (TFTs) [1] and optoelectronic devices [2], and they have been characterized by their higher drive current besides their visible light transparency. The latter can be realized due to wider bandgap of the TCOs. The oxides of tin especially its dioxide (SnO_2) is a well-known TCO which had been demonstrated in the past to behaving as a n-type material [3]. However, monoxide phase of the tin oxide (SnO) which exhibits p-type character remained underdeveloped to some extent partly because of instability of the SnO and significantly lower hole mobility exhibited by the monoxide of tin [4].

Enhancement of electron and hole mobilities in tin oxide was demonstrated in the past due to dopant incorporation accounting its atomic radii [5] and suitable enthalpy of oxide formation within the sub-lattice of the tin oxide [6]. However, bipolarity due to the same isoelectronic dopant, which is essential for the development of high mobility complementary p-and n-FETs, was never explored for the tin oxide as could have been suitable for the development of TFTs for CMOS and displays; yet, p- and n-character of the tin oxide were investigated for its relatively unstable undoped SnO [7] and stable (undoped and doped) SnO_2 [8] - [9].

The impact of isoelectronic doping in tin oxide by germanium (Ge) has been investigated here by experiments and DFT simulation, while Ge belongs to same group in the periodic table as tin (group - IV). Isoelectronic doping by Ge was shown to impact compressive strain in lattice leading to increased orbital overlaps between Sn 5s and Ge 5s, which were responsible for mobility increase of both carrier types.

II. Material Deposition Recipes

Ge doped tin oxide films were deposited on sapphire using RF co-sputtering and by using 99.99% pure germanium (Ge) and tin (Sn) targets. The power for the sputtering Sn target was fixed at 100 W, while variable power was used for the Ge target (from 0 to 20 W)-based on Ge atomic % needed in the films. The optimal p-type SnO_x:Ge [x = 1.17 – 1.42 based on XPS] was deposited due to O_2 flow rate [$O_2/(O_2+Ar)$] of 4.33%, while n-type SnO_2:Ge was obtained for $O_2/(O_2+Ar)$ = 12%. As-deposited films were annealed (post deposition anneal- PDA) in nitrogen (N_2) at 450°C for 1 hour. PDA films

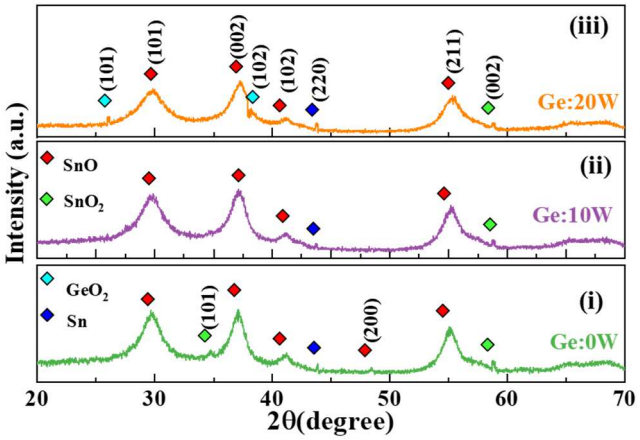

Fig.1. Measured XRD from post deposition annealed (PDA) p-type SnO_x:Ge deposited with different Ge target power (labelled - Ge: target power) [(i) Ge:0W (undoped) (ii) Ge:10W and (iii) Ge:20W]

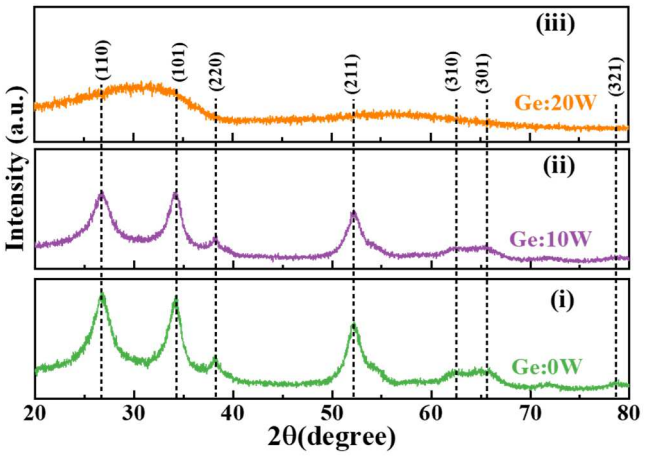

Fig.2. Measured XRD from post deposition annealed (PDA) n-type SnO_2:Ge deposited with different Ge target power (labelled - Ge: target power) [(i) Ge:0W (undoped) (ii) Ge:10W and (iii) Ge:20W]

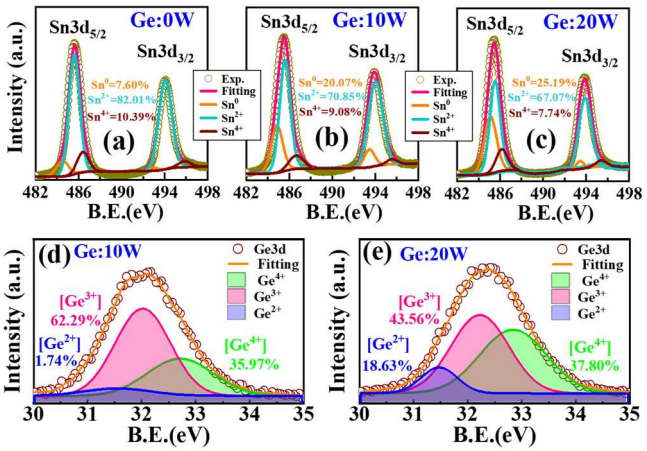

Fig. 3. Measured Sn 3d XPS from p-type SnO_x:Ge films fitted into Sn^{4+} (~486.6 and 495.9 eV), Sn^{2+} (~485.9 and 494.8 eV), and Sn^0 (~484.8 and 493.9 eV) spectroscopic peaks (a) Ge:0W (b) Ge:10W, and (c) Ge:20W. XPS of Ge 3d from SnO_x:Ge films further deconvolved into Ge^{2+} (~31.40 eV), Ge^{3+} (~32.20 eV) and Ge^{4+} (~32.80 eV) (d) Ge:10W, and (e) Ge:20W

were designated as Ge:0W, Ge:10W, and Ge:20W, based on the Ge target power that had been employed at the time of sputtering.

III. Results And Validation By DFT Simulation

Fig. 1 shows the XRD of SnO_x:Ge for different Ge power, demonstrating (101), (002), (102), (200), and (211) crystal planes of SnO. Higher Ge doping (Ge:20W) broadened FWHM of some SnO peaks which could be due to GeO_2 phase. For the optimized $O_2/(O_2+Ar)$ = 12% we instead observed a dioxide phase of the tin (SnO_2:Ge), and the respective XRD (Fig. 2) shows prominence of (110), (101), (220), (211), (310), (301), and (321) crystal planes of tetragonal SnO_2. The isoelectronic dopant effect by the Ge (i.e., same valency of dopant and substitutional site) was assessed via the XPS. Spectroscopic peak deconvolution of Sn 3d into Sn^0, Sn^{+2} and Sn^{+4} (Fig. 3) shows a significant decrease of Sn^{+2} (from 82–67.07%) versus Ge power for $\lceil O_2/(O_2+Ar)\rceil$ = 4.33%, while a decrease in Sn^{+4} is observed (from 73.5–60.8% - Fig. 4) for $O_2/(O_2+Ar)$ = 12% showing Ge^{+2} substitution for the former and Ge^{+4} substitution for the latter recipe to the respective tin vacant sites of same valencies. Tin

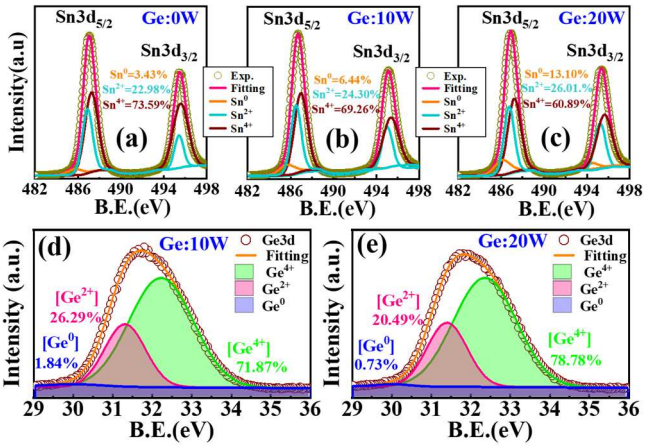

Fig. 4. Measured Sn 3d XPS from n-type SnO_2:Ge films deconvolved into Sn^{4+} (~486.9 and 496.1 eV), Sn^{2+} (~486.6 and 495.7 eV), and Sn^0 (~485.8 and 494.8 eV) spectroscopic peaks (a) Ge:0W (b) Ge:10W and (c) Ge:20W. Deconvolved Ge 3d from SnO_2:Ge films into Ge^0 (~29.78 eV), Ge^{2+} (~31.39 eV) and Ge^{4+} (~32.50 eV) (d) Ge:10W, and (e) Ge:20W

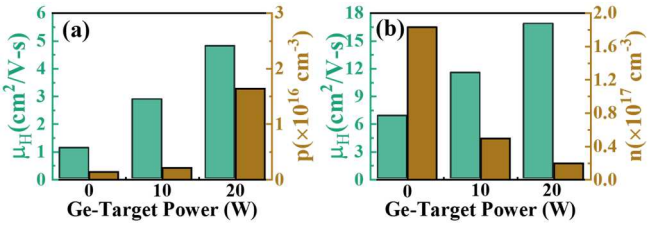

Fig. 5. Measured Hall mobility (μ_H) and carrier concentration (p: hole, n: electron) versus the Ge target power (a) p-SnO_x:Ge and (b) n-SnO_2:Ge

vacant sites could be created due to lower formation enthalpies of SnO (-281 kJ/mol) and SnO_2 (-531.8 kJ/mol) and they could dissociate during PDA leaving behind tin vacant sites and Sn^{+2} or Sn^{+4} cations at the interstitials. Increases of Sn^0 were observed versus Ge power for both the $\lceil O_2/(O_2+Ar)\rceil$ recipes (Figs. 3 - 4) representing a reduction mechanism at the interstitial sites by the electrons that were resulted by Ge atoms ionizing to either Ge^{+2} or Ge^{+4}.

Further deconvolution of Ge 3d spectroscopic peaks into the

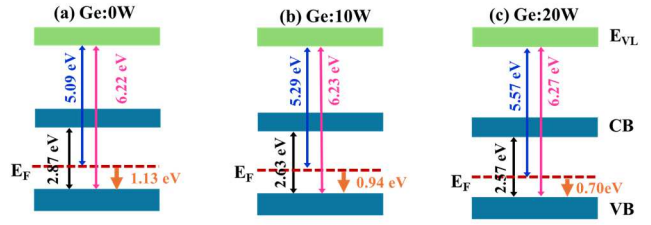

Fig.6. UV-photoemission spectroscopy (UV-PES) and UV-visible spectroscopy assessed energy band diagrams of SnO_x:Ge showing conduction band (CB), E_G, and valance band (VB) maximum and the work function with respect to the reference vacuum level (E_{VL}). Energy offsets between the Fermi energy level (E_F) and VBM are shown (a) Ge:0W, (b) Ge:10W and (c) Ge:20W

possible oxidation states (least χ^2 fits) corroborates our hypothesis since Ge^{+2} was found to be significantly increasing (Fig. 3) for $\lceil O_2/(O_2+Ar)\rceil$ = 4.33%, and on the other hand Ge^{+4} was found to be increasing for $\lceil O_2/(O_2+Ar)\rceil$ = 12% (Fig. 4). The presence of SnO_2 for $\lceil O_2/(O_2+Ar)\rceil$ = 12 % and SnO for $\lceil O_2/(O_2+Ar)\rceil$ = 4.33% corroborates as to n- and p-type characters of the films which was further validated through the Hall measurements (Fig. 5(a)-(b)). Remarkably, Hall mobility (μ_H) was increased due to Ge doping for both the cases. However, concentrations of n and p showed a reverse trend (Fig. 5). Electron concentration reduces with Ge doping due to higher formation enthalpy of stable GeO_2 (-580 kJ/mol) than SnO_2 (-531.8 kJ/mol) which does not allow O_2 to leave the lattice site for the oxygen vacancy (donor site) formation. Fermi energy level (E_F) versus Ge doping for the SnO_x:Ge

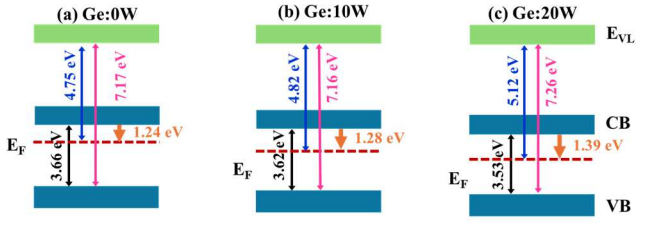

Fig.7. UV-photoemission spectroscopy (UV-PES) and UV-visible spectroscopy assessed energy band diagrams of SnO_2:Ge showing conduction band (CB), E_G, and valance band (VB) maximum and the work function with respect to the reference vacuum level (E_{VL}). Energy offsets between the Fermi energy level (E_F) and CBM are shown (a) Ge:0W, (b) Ge:10W and (c) Ge:20W

Effective Mass	Ge:0W	Ge:10W	Ge:20W
$m_h^*(\times m_0)$	0.621	0.601	0.597
$m_e^*(\times m_0)$	0.41	0.39	0.38

Table - I. DFT simulated effective masses of hole (m_h^* for SnO_x:Ge) and electron (m_e^* for SnO_2:Ge)

films (Fig. 6) was measured by UV-PES and E_F was found to be nearer the VBM as contrary to how E_F behaves in SnO_2:Ge films (E_F moves away from the CBM – see, Fig. 7).

Especially for the interpretation of μ_H increase for both the

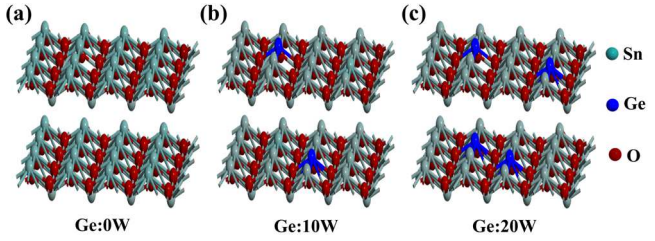

Fig. 8. Optimized geometric crystal structure with GGA correlation functional at 3 × 3 × 2 supercell of p-type SnO_x:Ge (a) Ge:0W, (b) Ge:10W, and (c) Ge:20W

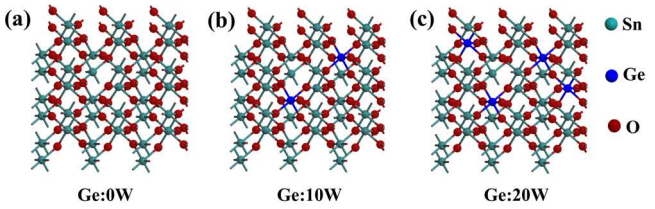

Fig. 9. Optimized geometric crystal structure with GGA correlation functional at 3 × 3 × 2 supercell of n-type SnO_2:Ge (a) Ge:0W, (b) Ge:10W, and (c) Ge:20W

carrier types versus Ge doping DFT simulations (Synopsis - QuantumATK®) were conducted for both SnO_x:Ge and SnO_2:Ge films. SnO (space group P4/nmm) and tetragonal SnO_2 (space group P2/mnm) were simulated, and relative Ge doping to experiment (assessed by XPS signals measured on the PDA films) was introduced by substituting the Sn atoms. The unit cells of SnO and SnO_2 were designed with (a=b=3.89 Å and a=b=4.76 Å respectively) and c/a ratio were 1.271 and 0.674 respectively. Their molecular structures with 3×3×2 repetition (Figs. 8 - 9) were then optimized and simulated

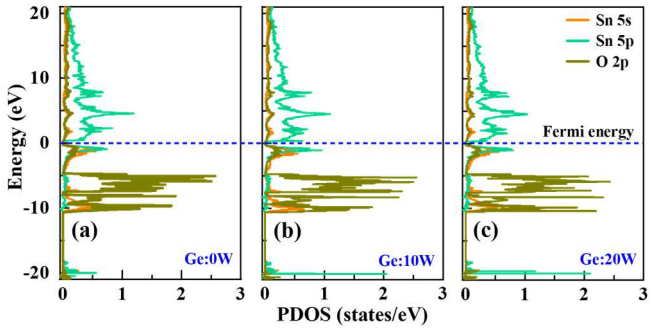

Fig. 10. (a)- (c) QuantumATK® simulated partial density of states (PDOS) of Sn 5s, Sn 5p and O 2p for p-type SnO_x:Ge for different Ge target power

using a linear combination of atomic orbitals (LCAO) calculator. Perdew–Burke–Ernzerhof (PBE) exchange-correlation, generalized gradient approximation (GGA), and pseudo potential method [projector-augmented wave (PAW)]. The density mesh cut-off in LCAO was set to 125 Hartree with broadening parameter of 300K for SnO_x:Ge, and 1000K for

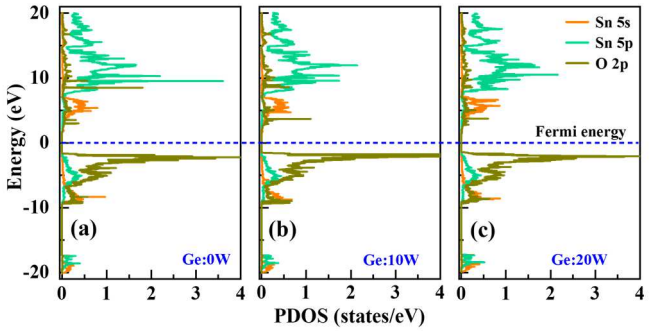

Fig. 11. (a)- (c) QuantumATK® simulated partial density of states (PDOS) of Sn 5s, Sn 5p and O 2p for n-type SnO_2:Ge for different Ge target power

SnO_2:Ge respectively and 7×7×1 sampling grid was taken. Both indirect and direct band edges were found for the SnO_x:Ge. However, direct band at the Γ-point was found to be better aggregable with the optical bandgap (E_G) values that were determined by the UV-Vis spectroscopy performed on the PDA SnO_2:Ge films (not shown). Fig. 10 (a) – (c) and Fig. 11 (a) – (c) show DFT simulated orbital contributions to the partial density of states (PDOS) of SnO_x:Ge and SnO_2:Ge respectively. Earlier it was reported that Sn 5s and O 2p orbitals in SnO [10] and Sn 5s and O 2s orbital in SnO_2 have their dominant roles to the respective p and n type characters [11]. While both Sn 5s and O 2p were found to contribute to the valance corroborating p-type character of SnO_x:Ge, yet Sn 5s was found to be outweighing to make the conduction band structure of SnO_2:Ge. We could not find a substantial role for O 2s in this regard.

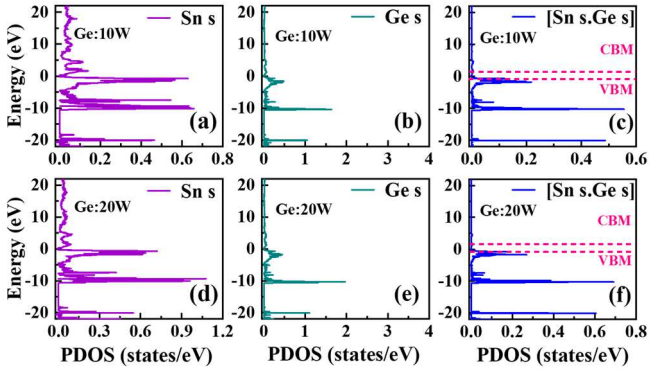

Fig. 12. QuantumATK® simulated partial density of states (PDOS) of Sn s, Ge s, and their overlap (scalar product) in energy (Sn s.Ge s) for p-type SnO_x:Ge; (a)–(c) Ge:10W and (d)–(f) Ge:20W

Table – I shows DFT simulated electron (m_e^*) and hole effective masses (m_h^*) and both were found to be reducing with higher Ge doping. m_h^* was found to be varying along the Γ→X, Γ→R and Γ→Z valleys in the E-k of the SnO_x:Ge. Thus, it was taken at Γ→Z where E_G was simulated to be the lowest, although E_G did not exactly match with the experiments. It could be due to error in the estimation by gradient approximation which was involved for DFT. m_e^* was rather determined at the Γ-point for SnO_2:Ge since its measured E_G was found to be well correlated at the corresponding k-point. Note that, by default, QuantumATK® uses a 5-point finite difference (FD)-based central stencil with a distance of 0.001 $Å^{-1}$ between the each k-point while approximating the double derivative for m^* calculation.

The decrease of effective masses of both the carrier types led to an increase of their mobilities, and Ge doping

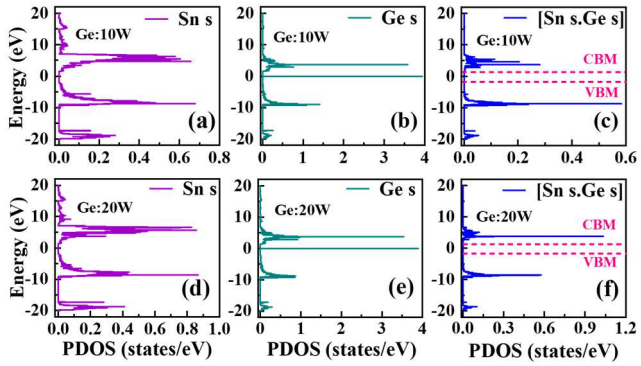

Fig. 13. QuantumATK® simulated partial density of states (PDOS) of Sn s, Ge s, and their overlap (scalar product) in energy (Sn s.Ge s) for n-type SnO_2:Ge; (a)–(c) Ge:10W and (d)–(f) Ge:20W

unequivocally had a role in it. DFT simulated PDOS of Sn s and Ge s while plotted in expanded scales for the optimized SnO_x:Ge (Fig. 12) and SnO_2:Ge (Fig. 13) show their increased overlaps (Sn s. Ge s) near the VBM and CBM respectively, and it explains the rationale of such mobility increase with Ge doping. Higher orbital overlap (Sn s. Ge s) could be resulted due to increased compressive strain in the tin oxide host lattice because of the Ge doping [12], which was determined from the WH fitting of the XRD data as were obtained for both the doping recipes (SnO_x:Ge and SnO_2:Ge) [not shown here]. Earlier it was claimed but in a different context of hole mobility increase by O_2 partial pressure control at the time of SnO deposition that increased tin in the host lattice could be helpful especially for mobility increase of the holes because of orbital delocalization near the VBM [13]. For both the recipes tin (Sn^0) was found to be increasing because of possible reduction mechanism at the interstitial sites as we discussed earlier with the context of XPS data (Figs. 3 – 4). Hence, principally it could also have a role for the observed hole mobility increase with Ge doping.

IV. Conclusion

Isoelectronic Ge doping in SnO_x and SnO_2 sizably increases orbital overlap between the Sn s and Ge s remarkably impacting hole and electron mobilities in the Ge doped tin oxide films. The proposed doping recipes were optimized and their favorable process impact on the carrier mobilities was further validated by comprehensive set of experiments and related DFT simulation.

Acknowledgment

JS and SG gratefully acknowledge the Prime Minister's Research Fellowship (PMRF), Govt. of India

References

[1] E. Fortunato, P. Barquinha, and R. Martins, "Oxide semiconductor thin-film transistors: a review of recent advances," Adv. Mater, vol. 24, pp. 2945–2986, May 2012, doi:10.1002/adma.201103228

[2] X. Yu, T. J. Marks, and A. Facchetti, "Metal oxides for optoelectronic applications," Nature materials, vol. 15, no. 4, pp. 383-396, Apr. 2016, doi: 10.1038/NMAT4599

[3] T. Zhang, Y. F. Wei, C. S. Zhang, G. He, T. J. Li, and D. Lin, "High-Performance Tin Oxide Thin-Film Transistors Realized by Co doping and Their Application in Logic Circuits," ACS Appl. Mater. Interfaces, vol. 16, no. 28, pp. 36577–36585, Jul. 2024, doi: 10.1021/acsami.4c05059

[4] S. Sheng, G. Fang, C. Li, S. Xu, and X. Zhao, "p-type transparent conducting oxides," *Phys. Status Solidi A*, vol. 203, no. 8, pp. 1891–1900, Jun. 2006, doi:10.1002/pssa.200521479

[5] W. Guo, L. Fu, Y. Zhang, K. Zhang, L.Y. Liang, Z.M. Liu, H.T. Cao, and X.Q. Pan, "Microstructure, optical, and electrical properties of p -type SnO thin films," Appl. Phys. Lett., 96(4), 042113, 2010

[6] J. Yang, Z. Yang, T. Meng, Y. Han, X. Wang, and Q. Zhang, "Effects of silicon doping on the performance of tin oxide thin film transistors," Phys. Status Solidi A, vol. 213, no. 4, pp. 1010–1015, Apr. 2016

[7] S. J. Lee, Y. Jang, H. J. Kim, E. S. Hwang, S. M. Jeon, J. S. Kim, T. Moon et al, "Composition, microstructure, and electrical performance of sputtered SnO thin films for p-type oxide semiconductor," *ACS applied materials & interfaces*, vol. 10, no. 4, pp. 3810-3821, Jan. 2018, doi: 10.1021/acsami.7b17906.

[8] D. Liang, B. Chen, B. Feng, Y. Ikuhara, H. J. Cho, and H. Ohta, "Optimization of two-dimensional channel thickness in nanometer-thick SnO_2-based top-gated thin-film transistors using electric field thermopower modulation: implications for flat-panel displays," *ACS Applied Nano Materials*, vol. 3, no. 12, pp. 12427-12432, Dec. 2020, doi:10.1021/acsanm.0c03069

[9] Y. F. Wei, T. Zhang, J. J. Wu, T. J. Li, and D. Lin, "Mobility enhancement of tin oxide thin-film transistor by indium-doping." *Vacuum*, vol. 221, pp. 112868, Dec. 2024, doi:10.1016/j.vacuum.2023.112868

[10] A. Togo, F. Oba, I. Tanaka, and K. Tatsumi, "First-principles calculations of native defects in tin monoxide," *Physical Review B*, vol. 74, no. 19, pp. 195128, Nov. 2006, doi:10.1103/PhysRevB.74.195128

[11] X. Cai, P. Zhang, and S. H. Wei, "Revisit of the band gaps of rutile SnO_2 and TiO_2: a first-principles study," *Journal of Semiconductors*, vol. 40, no. 9, pp. 092101 Jun. 2019, doi:10.1088/1674-4926/40/9/092101

[12] J. Singh, S. Gora, M. Jangra, and A. Datta, "Germanium Doped SnO_2: An Exploratory Channel Material for High On–Off Current Ratio and Low Subthreshold Slope in n-Type SnO_2: Ge Thin Film Transistor," *IEEE Transactions on Electron Devices*, vol. 72, no. 1, pp. 282-288, Jan. 2025, doi:10.1109/TED.2024.3510237

[13] J. A. Caraveo-Frescas, P. K. Nayak, H. A. Al-Jawhari, D. B. Granato, U. Schwingenschlögl, and H. N. Alshareef, "Record Mobility in Transparent p-Type Tin Monoxide Films and Devices by Phase Engineering," ACS Nano, 7 (6), 5160-5167, 2013